Full length article

Valence electron concentration as an indicator for mechanical properties in rocksalt structure nitrides, carbides and carbonitrides

Karthik Balasubramanian [a], Sanjay V. Khare [b], Daniel Gall [c, *]

[a] Department of Mechanical, Nuclear and Aerospace Engineering, Rensselaer Polytechnic Institute, Troy, NY 12180, USA
[b] Department of Physics and Astronomy, The University of Toledo, 2801 West Bancroft Street, Toledo, OH 43606, USA
[c] Department of Materials Science and Engineering, Rensselaer Polytechnic Institute, Troy, NY 12180, USA

ARTICLE INFO

ABSTRACT

First-principles calculations are employed to determine the mechanical properties of rock-salt structure binary and ternary transition metal nitrides, carbides, and carbonitrides from groups 4 to 12, predicting a unified indicator for mechanical properties: the valence electron concentration (VEC). Pugh's and Poisson's ratios indicate an increasing ductility with increasing VEC, with a brittle-to-ductile transition at a critical VEC = 10. The calculated C_{44} of carbonitrides and ternary nitrides monotonically decreases from 164 ± 12 GPa at VEC = 8 to -39 ± 46 GPa at VEC = 11, indicating a transition to mechanical instability at VEC = 10.6. Similarly, the average isotropic elastic modulus decreases slightly from 420 GPa for VEC = 8 to 388 GPa for VEC = 10, but then steeply to -98 GPa for VEC = 11, while the corresponding hardness decreases from 25 to 12 to 2 GPa. The overall softening with increasing VEC is attributed to the increasing electron density in $d-t_{2g}$ orbitals, which overlap upon shear and cause a decrease in C_{44}. Phonon dispersion curves, calculated at 0 K for binary nitrides and carbides, exhibit imaginary frequencies for VEC ≥ 10, indicating a dynamical stability-to-instability transition between VEC = 9 and 10, which is smaller than the critical VEC = 10.6 for the mechanical stability-instability transition. In addition, mechanical stability is increased by magnetic ordering but decreased when accounting for on-site Coulomb repulsion, while temperature and vacancies cause a reduction in the magnitude of C_{44} for both stable and unstable compounds, likely leading to an increase in the critical VEC for the stability-instability transition. The overall results indicate a narrow region between VEC = 9 and 10 where rocksalt carbonitrides are ductile but also exhibit a high hardness, mechanical and dynamical stability, and therefore are expected to exhibit the highest toughness.

© 2018 Acta Materialia Inc. Published by Elsevier Ltd. All rights reserved.

1. Introduction

Transition metal nitrides and carbonitrides are widely used as hard and protective coatings [1—10] and as diffusion barrier layers [11—14] due to their excellent thermal stability, mechanical properties, and corrosion resistance [1—4,10,15—18]. Many transition metal nitrides and carbonitrides crystallize in the rocksalt structure, including ScN [19], TiN [20], HfN [3], ZrN [21], VN [22], NbN [23], TaN [16], CrN [24], MoN [25], WN [26], FeN [27], NbC$_{1-x}$N$_x$ [2], TaC$_{1-x}$N$_x$ [28], VC$_{1-x}$N$_x$ [29], HfC$_{1-x}$N$_x$ [30], ZrC$_{1-x}$N$_x$ [31] and TiC$_{1-x}$N$_x$ [32]. The early transition metal nitrides, carbides and carbonitrides, particularly with metal elements of group 4, are well studied and

have excellent mechanical properties which are predicted to further improve with an increasing number of valence electrons [33,34], resulting in increased ductility and toughness when moving to the right in the periodic table [35—39]. However, large electron concentrations can lead to negative C_{44} values and a corresponding mechanical instability, as reported for example for rocksalt structure WN [40,41] and MoN [25,40,42]. This instability has been attributed to an increasing overlap and constructive interference of $d-t_{2g}$ orbitals upon shear, leading to an energy reduction during shear deformation and a mechanical instability of the cubic structure [41,43—45]. Correspondingly, the mechanical properties of rock-salt structure transition metal nitrides vary widely [15,17,46]. For example, the elastic modulus E decreases from theoretically calculated 450 GPa for TiN [33,47] to -285 GPa for WN [41], with intermediate values of 370 GPa for ZrN [33], 386 GPa for VN [35], 283 GPa for V$_{0.5}$W$_{0.5}$N [37], and experimental

* Corresponding author.
  E-mail address: galld@rpi.edu (D. Gall).

values measured by nanoindentation of 400 GPa for HfN [3] and 273 GPa for NbN [23]. Combining binary nitrides to form ternary and quaternary nitrides and/or extending the materials system to carbonitrides provides ample opportunities to optimize strength, ductility and toughness for a specific application. For this purpose, it is desirable to have a preliminary indictor for mechanical properties of transition metal nitrides and carbonitrides which provides guidance in the process of alloy design.

The valence electron concentration (VEC) is defined as the number of valence electrons per formula unit. This parameter has been reported to be a significant indicator of the structural, thermodynamic and mechanical properties of binary and ternary compounds in various materials systems, and has been used to predict the phase stability and relative formation enthalpy in high entropy alloys [48], the critical temperature of high temperature superconductors [49], elastic and electronic properties of alkaline earth tin oxides [50], bulk moduli for transition metal nitrides in the pyrite and fluorite phase [51], the stability and electronic structure in Mo-S-I nanowires [52], and the formation enthalpy in Y carbonitrides and boronitrides [53]. Similarly, tuning of the VEC to tailor mechanical properties has also been employed to transition metal carbonitrides. In particular, VEC = 8.4 has been predicted to yield a maximum strength in $TiC_{1-x}N_x$ alloys [44,45,54], while increasing VEC above 8.4 in transition metal nitrides and carbonitrides has been predicted to increase ductility and toughness [35,38,55], which may be associated with an increased overlap of $d-t_{2g}$ orbitals [35,38,56] and the reported decrease in the shear modulus [57]. VEC tuning has also been employed to enhance hardness in transition metal carbides and the $Nb_xZr_{1-x}N$ system by promoting nucleation of stacking faults and phase boundaries during synthesis and hindering dislocation motion across these faults and phase boundaries [58,59] and enhancing ductility of pseudo binary cubic $Ti_xW_{1-x}N$ alloys [60]. Furthermore, VEC tuning has also been employed to predict enhanced mechanical properties of Mo-Al-Cr-N alloys by varying the relative compositions of the components [61] and increasing the thermal stability of Ti-Al-N alloys by suitable Ta alloying [62]. These previous studies motivate a systematic study on the trends of all the elastic constants, moduli and hardness of transition metal carbonitrides in the rocksalt structure as a function of VEC, focusing particularly on brittle-to-ductile transitions and mechanical stability, with the overall goal to provide guidelines for designing tougher alloys.

In this work, we use *ab initio* calculations to identify trends in the mechanical properties of rock-salt structure transition metal nitrides and carbonitrides from groups 4 to 12. The valence electron concentration is demonstrated to be a key indicator for mechanical properties. Increasing the VEC leads to a decrease in Pugh's ratio and an increase in Poisson's ratio, indicating an increasing ductility with increasing VEC, and a brittle to ductile transition at VEC = 10. The shear elastic constant C_{44} decreases with increasing VEC, indicating a transition to mechanical instability for VEC >10.6. Similarly, the average calculated isotropic elastic modulus decreases from 426 to −83 GPa and the hardness decreases from 25 to 2 GPa with the VEC increasing from 8 to 11.

2. Computational procedure

First-principles density functional calculations were performed using the Vienna *ab initio* simulation package (VASP) [63,64], employing periodic boundary conditions, a plane wave basis set, the Perdew-Burke-Ernzerhof (PBE) generalized gradient approximation exchange correlation functional [65], and the projector-augmented wave method [66]. All computational parameters were chosen such that calculated total energy differences were converged to within 1 meV/atom. This included a 500 eV cut-off

energy for the plane-wave basis set expansion and a Γ-centered $20 \times 20 \times 20$ k-point grid for conventional unit cells containing 8 atoms for binary nitrides, carbides and carbonitrides. Special quasi-random structures (SQS) [67] were constructed for two ternary systems ($Ta_{0.25}W_{0.75}N$) and ($WC_{0.25}N_{0.75}$) using unit cells containing 32 cations and 32 anions, to check if random occupation of lattice sites would affect the general trends obtained using the 8 atom conventional unit cells. Pseudopotentials were chosen, following the recommendation by VASP for relatively accurate calculations, such that the following electrons were explicitly calculated (i.e. not included in the pseudopotential): 3s, 3p, 3d and 4s for the elements Ti and V; 3p, 3d and 4s for Cr and Mn; 3d and 4s for Fe to Zn; 4s, 4p, 4d and 5s for Zr to Mo; 4p, 4d and 5s for Tc to Rh; 4d and 5s for Pd to Cd; 5p, 5d and 6s for Hf to W; 5d and 6s for Re to Hg. Atomic positions and lattice parameters were relaxed until an energy convergence of 10^{-4} eV/atom was achieved. This was done by multiple calculations for each atomic configuration, where atoms were relaxed at a fixed lattice parameter that was varied for the different calculations by 0.01 Å increments. Subsequently, the relaxed lattice constant and corresponding energy was determined by fitting the calculated energy vs lattice parameter with a second order polynomial. The three independent elastic constants for cubic systems C_{11}, C_{12} and C_{44} were determined by applying a set of strains to the conventional unit cell, and fitting second order polynomial functions to the calculated elastic energy vs strain. In particular, C_{11} was determined from tensile and compressive ±1–3% strains along [001], C_{12} was calculated from the bulk modulus B using $C_{12} = (3B - C_{11})/2$ [68], where B was obtained from a fit of the calculated energy vs lattice constant using the Murnaghan equation of state, and C_{44} was determined using a 1–5% shear strain along [100]. For structures, which do not truly exhibit cubic symmetry, such as ternary systems, the elastic constants were averaged over the directions [69]. That is C_{11}, C_{22} and C_{33} was averaged to yield an average tensile elastic constant $\overline{C}_{11}$. Similarly, the shear elastic constants C_{44}, C_{55} and C_{66} were averaged to yield an average shear elastic constant $\overline{C}_{44}$. We note that these ternary systems could be referred to as pseudobinary alloys, as anti-site substitutions were not considered such that metal atoms always occupy cation sublattice sites while nitrogen and carbon atoms always occupy anion sublattice sites. We also note that DFT predictions of elastic constants have uncertainties associated with the choice of the exchange-correlation functional. The PBE functional used in our study has been reported to yield bulk moduli that deviate by 5–20% from experimental values for a large range of materials systems [70]. Correspondingly, we expect the elastic constants reported in our study to have an accuracy of 5–20%.

The isotropic elastic modulus E and isotropic shear modulus G were determined from the calculated elastic constants using Hill's approximation [71] calculated from Voigt and Reuss methods. We note here that while the Voigt and Reuss methods yield similar values for material systems with positive elastic constants, they vary considerably for systems with negative elastic constants. Pugh's ratio k and isotropic Poisson's ratio ν were calculated using $k = G/B$ and $\nu = (E/2G)-1$ [72]. Vicker's hardness was then calculated according to Tian's model $H_v = 0.92k^{1.137}G^{0.708}$ [73]. The dynamic stability of the carbides and nitrides was investigated by calculating the phonon-dispersion curves using PHONOPY [74] and looking for imaginary phonon modes. This was done by calculating the force constants and subsequently the phonon dispersion curves by displacing atoms along high symmetry directions in a 216 atom cell ($3 \times 3 \times 3$ supercell), using a $2 \times 2 \times 2$ k-point mesh. The mechanical properties in magnetic binary nitrides, MnN, CrN, CoN, FeN and NiN, were calculated by considering paramagnetic, ferromagnetic and antiferromagnetic ordering of the ions in the [100], [110] and [111] directions by constructing $2 \times 2 \times 2$ supercells containing 32

cations and 32 nitrogen atoms, using a $6 \times 6 \times 6$ k-point mesh. The site projected density of states was obtained by projecting the wave functions of each band onto local orbitals around each ion.

3. Results and discussion

Fig. 1 shows the calculated Pugh's ratio k and Poisson's ratio ν for rock-salt structure binary carbides and nitrides of transition metals from groups 4–12. Open and closed symbols denote carbides and nitrides, respectively, while the plotted symbol shape and color specify the row and column of the metal in the periodic table. Pugh's and Poisson's ratios are determined from the calculated elastic constants, as described in Section II. They are plotted because they are commonly used as an empirical indicator for a materials ductility [72]. More specifically, a material is expected to be ductile, if its Pugh's ratio k is below a critical value of 0.5–0.6 and its Poisson's ratio ν is above a critical value of 0.25–0.28 [72]. The plot in Fig. 1(a) of Pugh's vs Poisson's ratio indicates a strong correlation of these two parameters, with a nearly linear decrease in k with increasing ν. Linear curve fitting provides a slope of −2.7, which is close to the average slope of −2.6 for a perfectly isotropic material in the range $\nu = 0.2$–0.45, as deduced from $k = 1.5 \times (1-2\nu)/(1+\nu)$ and correspondingly $dk/d\nu = -4.5/(1+\nu)^2$ [72]. The dotted horizontal and vertical lines divide the plot into regions of ductile and brittle materials, using critical values of $k = 0.5$ and $\nu = 0.28$. The data points from group 4 nitrides and group 4 and 5 carbides are in the left top corner of Fig. 1(a), indicating that they are expected to be brittle. In contrast, nitrides of metals from group 5–12 and carbides of metals from group 6–12 are in the bottom right region, suggesting ductility. We attribute the increasing ductility with increasing VEC to a change from a more covalent bonding character to more metallic bonding. More specifically, carbides and nitrides in the early VEC region (that is VEC ~ 8) exhibit more directional covalent bonding associated with N 2p orbitals, while increasing VEC (up to 17) moves the Fermi level up to near the top of the metal d bands such that non-directional metallic bonding dominates the overall atomic bonding, leading to an increased ductility. In addition, comparing k and ν for nitrides and carbides with the same VEC in the range of 8−11 suggests that carbides are slightly more brittle than nitrides, which may be attributed to the stronger covalent bonding character for the carbides.

The binary nitrides and carbides that are predicted to be brittle, all have a VEC of 8 or 9, while the compounds that are in the ductile region have a VEC of 10−17. In fact, the data from the left top to the right bottom approximately corresponds to an increasing VEC, as indicated by the arrow in Fig. 1(a). This implies that increasing the valence electron concentration results in improved ductility, which is in good agreement with previous reports [17,38,55]. In addition, the data indicates a brittle-to-ductile transition, which occurs for both carbides and nitrides at the same VEC ≈ 10. This suggests that the VEC is a key parameter for classifying the mechanical properties of rocksalt structure carbides and nitrides. Correspondingly, we directly plot in Fig. 1(b) and (c) the Pugh's and Poisson's ratios as a function of VEC.

Pugh's ratio k, plotted in Fig. 1(b) as a function of VEC, decreases steeply when moving to the right in the periodic table, from an average of 0.64 for group 4 nitrides at VEC = 9 to $k = 0.14$ for CrN at VEC = 11, and similarly from an average of 0.74 for group 4 carbides at VEC = 8 to $k = 0.16$ for group 8 carbides at VEC = 12. Pugh's ratio does not have a valid value for group 6−9 nitrides (with the exception of CrN and CoN) and for group 7−9 carbides (with the exception of MnC, FeC, RuC and CoC), because the calculated C_{44} values for these compounds are negative. For VEC >12, Pugh's ratio remains approximately constant and reaches an average $k = 0.28$
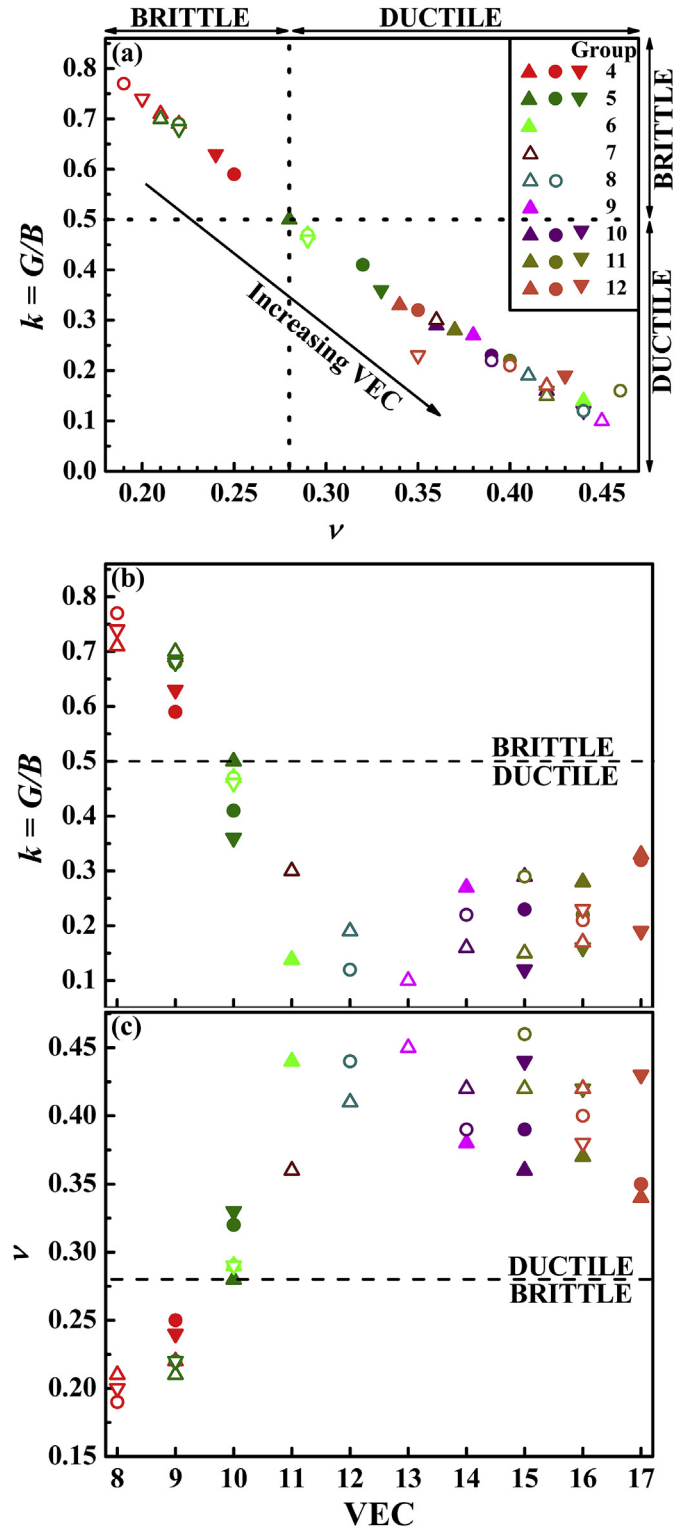
Fig. 1. Pugh's ratio $k = G/B$ and Poisson's ratio ν of transition metal nitrides (solid symbols) and carbides (open symbols) from group 4 to 12 and rows IV, V and VI (up triangles, circles, down triangles) of the periodic table. The ductile and brittle regions are indicated in plots of (a) k vs ν, (b) k vs the valence electron concentration VEC, and (c) ν vs VEC. A table of the plotted numerical values is provided as supplementary material.

and 0.21 for group 12 nitrides and carbides with VEC = 17 and 16, respectively. Poisson's ratio ν, as plotted in Fig. 1(c), exhibits a similar but inverse dependency on VEC. More specifically, ν

increases steeply from an average of 0.20 for group 4 carbides at VEC = 8 to $\nu = 0.44$ for VEC = 12, and remains relatively constant for VEC >12 to reach 0.38 and 0.41 for group 12 nitrides and carbides at VEC = 17 and 16, respectively. Both Pugh's and Poisson's ratios indicate a brittle-to-ductile transition at a VEC $\approx$ 10. This is in good agreement with previous reports of nitrides which suggest a brittle character and cracking at failure for group 4 and 5 nitrides (VEC <10) [35–37] while carbonitrides with VEC > 10 exhibit comparatively more ductility [35–37]. In addition, we note that ternary carbonitrides (pseudobinary alloys) exhibit more ductility than the binary carbides/nitrides at the same VEC. This can be attributed to the fact that in a ternary alloy, the bonds are dissimilar resulting in less symmetric bond relaxation and thus more plastic deformation [36,38,39,55].

An alternative indicator for the ductility of a material is the Cauchy pressure $p_C = C_{12} - C_{44}$ [75], where $p_C < 0$ typically indicates a brittle material and correspondingly $p_C > 0$ classifies a material as ductile. The calculated p_C values of the binary carbides and nitrides are provided in the supplementary document. They are positive for all mechanically stable nitrides and carbides from groups 6–12, but are negative for carbides of metals from groups 4 and 5. Thus, the calculated p_C values suggest that all nitrides are ductile, while carbides with VEC $\leq$9 are brittle and carbides with VEC $\geq$10 are ductile. The latter result on carbides is in perfect agreement with the above analysis using ν and k. We note, that nitrides with VEC = 9 have positive but relatively small Cauchy pressures of 5, 38, and 43 GPa, suggesting that they are "ductile" but relatively close to brittle. That is, they are more ductile than the carbides with the same VEC, which is attributed to the larger radius of nitrogen vs carbon, and a correspondingly smaller covalent bonding character in the nitrides. This is also consistent with the larger average $\nu = 0.24$ for nitrides with VEC = 9 than $\nu = 0.20$ for carbides with VEC = 9. We note that another parameter that indicates a materials ductility has recently been introduced: The cooperation parameter δ. It is primarily applied to characterize the ductility of metallic glasses [76] and classifies materials as ductile if $\delta > 1$, corresponding to a value of $\nu > 0.31$. However, the parametric values of $k < 0.5$ and $\nu > 0.28$ are more commonly used for transition metal nitrides and carbides and are therefore used in this article.

Fig. 2 is a plot of the calculated single crystal shear modulus C_{44} for group 4 to 12 transition metal nitrides and carbides as a function of valence electron concentration. The C_{44} of the nitrides decreases steeply from an average of 136 GPa for group 4 nitrides (VEC = 9) to −148 GPa for group 7 nitrides (VEC = 12) and increases again to averages of −39, 54, 39 and 46 GPa for group 9, 10, 11 and 12 nitrides (VEC = 14–17). In addition, for each fixed VEC corresponding to a specific column in the periodic table, C_{44} decreases when moving down from row IV to V to VI. The nitrides with VEC = 11–14 have negative C_{44} values (with the exception of CrN and CoN with small C_{44} = 8 and 55 GPa, respectively, which may be an artifact of our calculations that neglect Coulomb repulsion, as discussed later). The negative C_{44} indicates mechanical instability of the rock-salt structure for these nitrides. The carbides show a similar trend as the nitrides, with C_{44} decreasing for the early transition metals from an average of 164 GPa for group 4 carbides to −9 GPa for group 7 carbides (VEC = 11) and to a minimum of −47 GPa at VEC = 13, followed by an increase to 47 and 22 GPa for group 10 and 12 carbides. Negative C_{44} values for VEC = 11–13 indicate a region of mechanical instability. However, all row-four carbides, including MnC, FeC, and CoC, as well as RuC from row V with VEC = 12, exhibit positive C_{44} which may be attributed to the localization of electrons as discussed below. We note that PtC and AuC with VEC = 13 and 14 have positive C_{44} = 19 and 36 GPa values, despite that they belong to groups 9 and 10. However, they are nevertheless mechanically unstable because their $C_{11} < C_{12}$. It is also imperative to mention here that some nitrides (such as CrN [24,77–80], MnN [81] and FeN [82]) and carbides such as (CrC [83] and MnC [84]) exhibit magnetic character. Of these magnetic compounds, CrN is the most important as it falls in the valence electron region of interest − that is near mechanical instability. CrN at 0 K is most stable in the antiferromagnetic orthorhombic structure [24,77,79,80,85–87], but attains a paramagnetic rocksalt structure near room temperature [77,79]. For the sake of analyzing the trends in mechanical properties, all nitrides and carbides in this investigation are considered non-magnetic and in the rocksalt structure unless indicated otherwise.

We briefly discuss here the mechanical stability/instability as evidenced by positive/negative C_{44} values of rocksalt phases in Fig. 2. Both nitrides and carbides exhibit a transition to mechanical instability with increasing valence electron concentration at approximately VEC = 11, and a return to stability around VEC = 14. The instability range is slightly smaller for the carbides than the nitrides, and the C_{44} values are less negative. This can be attributed to the higher covalency of metal-carbon bonds which are facilitated by the hybridization of metal $d-e_g$ and non-metal p orbitals, resulting in a stronger resistance to shear which leads to higher C_{44} values for the carbides than the corresponding nitrides, as plotted in Fig. 2. The decrease in C_{44} and the onset of mechanical instability at VEC = 11 can be explained by the overlap of $d-t_{2g}$ orbitals which increases upon shear, resulting in an energy reduction during shearing of compounds with partially filled $d-t_{2g}$ orbitals [41,43,44,88]. Correspondingly, we propose that the reason for returning back to mechanical stability for group 10–12 nitrides and carbides is due to both bonding and anti-bonding d–orbitals being nearly full, such that the additional overlap of $d-t_{2g}$ orbitals which increases the split between these orbitals has a negligible energy benefit upon shearing. This can be more quantitatively understood by analyzing the partial electron occupancies of the $d-t_{2g}$ orbitals and $d-e_g$ orbitals, which are calculated by projecting the wavefunction onto local orbitals as described in Section II. The fraction of 5d-electrons that occupy $d-t_{2g}$ orbitals for the nitrides from group 4–12 and period VI varies as 0.62, 0.66, 0.68, 0.69 0.71, 0.69, 0.68, 0.63 and 0.61 for HfN, TaN, WN, ReN, OsN, IrN, PtN, AuN and HgN, respectively, indicating a monotonic increase from 0.62 for HfN
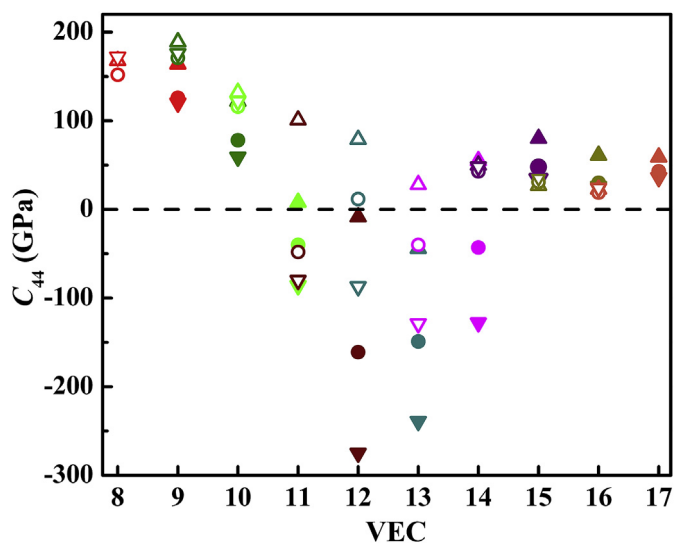
Fig. 2. Plot of the single crystal shear modulus C_{44} as a function of valence electron concentration for transition metal nitrides and carbides from group 4 to 12. Symbol shapes and colors are as in Fig. 1. A table with the numerical values is provided as supplementary material. (For interpretation of the references to color in this figure legend, the reader is referred to the Web version of this article.)

(group 4) to 0.71 for OsN (group 8) followed by a monotonic decrease to 0.61 for HgN (group 12). This trend is reflected in the plotted C_{44}, which decreases from group 4 to 8 and increases again to group 12, suggesting that a large fractional occupation of $d-t_{2g}$ orbitals yields a low (or even negative) resistance against shear, with the lowest values of $C_{44} = -275$ GPa for ReN of group 7, at VEC of 12, and $C_{44} = -239$ GPa for OsN of group 8, at VEC of 13, which has the highest fraction of d electrons occupying $d-t_{2g}$ orbitals.

Fig. 3 is a plot of the average single crystal shear modulus $\overline{C}_{44} = (C_{44} + C_{55} + C_{66})/3$ for carbonitrides and ternary nitrides using group 4 to 6 transition metals. These calculations are done to explore in more detail the dependence of $\overline{C}_{44}$ on VEC for VEC smaller than 11, and to quantify the critical VEC for the transition to mechanical instability. The plot includes carbonitrides from all nine group 4 to 6 transition metals which are formed using a rock-salt type structure with, however, a mixture of carbon or nitrogen atoms occupying the four anion sites of a conventional unit cell, such that 0, 25, 50, 75, or 100% of anions are carbon and the remainder nitrogen. Similarly, the six sets of ternary metal alloy nitrides presented in Fig. 3 are all those that contain two transition metals from the same period and adjacent groups, that is group 4 and 5 or group 5 and 6. All plotted data sets contribute to an overall well defined trend of $\overline{C}_{44}$ vs VEC, indicating an approximately parabolic curve. The average $\overline{C}_{44}$ of carbonitrides of group 4 increases slightly from an average of 164 GPa for group 4 carbides at VEC = 8 to 178 GPa at VEC = 8.25, but then decreases steeply to 134 GPa for group 4 nitrides at VEC = 9. Thus, $\overline{C}_{44}$ reaches a maximum at VEC ~8.25, in agreement with previous reports which indicate a maximum strength of $TiC_{1-x}N_x$ alloys at VEC = 8.4 [44,45], and an increasing ductility and toughness for VEC increasing above 8.4 for transition metal nitrides and carbonitrides [35,38,55]. The calculated $\overline{C}_{44}$ of the carbonitrides and ternary nitrides continues to decrease steeply with increasing VEC >9, reaching an average of 45 GPa for the ternary carbonitrides and nitrides of metallic alloys at VEC = 10.5 and an average $\overline{C}_{44} = -39$ GPa for group 6 nitrides at VEC = 11. This negative value indicates mechanical instability at VEC = 11. Linear interpolation of the $\overline{C}_{44}$ data sets of carbonitrides and ternary nitrides in the VEC = 10–11 region indicates that $\overline{C}_{44} = 0$ for VEC = 10.74 for $MoC_{1-x}N_x$, 10.72 for $WC_{1-x}N_x$, 10.48 for $Nb_{1-x}Mo_xN$ and 10.46 for $Ta_{1-x}W_xN$. Correspondingly, the average critical VEC that leads to mechanical instability is 10.6 ± 0.2. All calculated

carbonitrides and ternary nitrides of Cr with VEC = 10–11 have positive $\overline{C}_{44}$ values and are not considered here for the calculation of the critical VEC for mechanical instability. The trend of a decreasing $\overline{C}_{44}$ with increasing VEC is consistent with previous theoretical reports which report a similar decrease in $\overline{C}_{44}$ with increasing VEC [89–93].

Special quasi-random structure calculations of two specific ternaries, $Ta_{0.25}W_{0.75}N$ and $WC_{0.25}N_{0.75}$, yield $\overline{C}_{44} = -10$ and -6 GPa, respectively, in good agreement with previous studies which report a $\overline{C}_{44}$ of ~ -15 GPa for $Ta_{0.25}W_{0.75}N$ [90]. These two compositions both have a VEC = 10.75 and are chosen because they are near the mechanical stability-instability transition. The data points are also plotted as black open symbols in Fig. 3 at VEC = 10.75. The values are slightly higher (by 12 and 9 GPa) than the $\overline{C}_{44} = -22$ and -15 GPa obtained using the 8 atom unit cells for the same compositions. This suggests that disorder has only a minor effect on the calculated VEC for transition to mechanical instability. The approximately 10 GPa higher values from the SQS calculations indicate that random occupation on cation or anion sites mechanically stabilizes the rocksalt structure. This leads to a slight increase in the expected critical VEC for the stability-instability transition. More quantitatively, using the average slope $d(\overline{C}_{44})/d(VEC) = 183$ GPa we estimate a correction of $+0.05$. However, this correction is smaller than the above stated uncertainty, such that we retain a value of VEC = 10.6 ± 0.2 for the stability-instability transition.

Fig. 4(a) shows the bulk modulus B as a function of VEC for the same carbonitrides and ternary nitrides discussed above, using group 4 to 6 transition metals. The plot indicates that the different ternary nitrides and carbonitrides with the same VEC exhibit similar B values, typically within a range of ~50 GPa. B increases approximately linearly from an average of 255 GPa for VEC = 8 to $B = 314$ and 360 GPa for VEC = 9 and 10, but remains approximately constant for VEC >10, with an average of 366 GPa for VEC = 11. These values are in reasonable agreement with previously published bulk moduli of binary carbides and nitrides, with predicted averages of 234, 286, 330 and 334 GPa for VEC = 8, 9, 10 and 11, respectively [94].

The plot of the tensile elastic constant $\overline{C}_{11} = (C_{11} + C_{22} + C_{33})/3$ vs VEC in Fig. 4(b) indicates an initial steep increase from an average of 499 GPa for group 4 carbides with VEC = 8 to 579 GPa for group 4 nitrides with VEC = 9. However, the data for VEC >9 shows large variations in $\overline{C}_{11}$ for different nitrides and carbonitrides with the same VEC, leading to the rather noisy data in Fig. 4(b) and no evident trend of $\overline{C}_{11}$ vs VEC > 9. That is, in contrast to $\overline{C}_{44}$ which is a strong function of the VEC as shown in Fig. 3, the VEC is a less useful parameter in determining $\overline{C}_{11}$ of the investigated nitrides and carbonitrides. This is consistent with previous reports which indicate an increase in the tensile elastic constant $\overline{C}_{11}$ with increasing VEC from 8 to 10, and a subsequent decrease to group 6 nitrides with VEC = 11 [89–93]. We note here that elastic constants of the ternary nitrides, carbides and carbonitrides can also be strongly affected by atomic ordering. Some carbides and nitrides have been reported to exhibit ordering on the metal sublattice [95–97] to form more thermodynamically stable structures. Vacancy ordering on the non-metal sublattice has also been observed for some carbides [98,99]. Both short range or long range ordering has the potential to affect the elastic constants. However, a systematic study of ordering effects is beyond the scope of this study, since it not only requires large-cell SQS calculations but also relaxation of the cubic symmetry into less symmetric e.g. rhombohedral ordered structures.

Fig. 5(a) is a plot of the isotropic elastic modulus E of carbonitrides and ternary nitrides vs VEC, as determined from the elastic constants presented in Figs. 3 and 4. E increases slightly from an
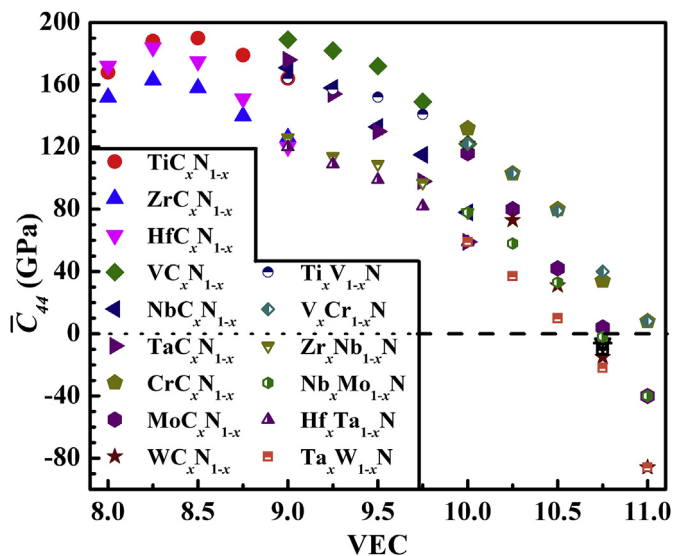
Fig. 3. The symmetric single crystal shear modulus $\overline{C}_{44}$ as a function of valence electron concentration VEC for transition metal carbonitrides and ternary nitrides.
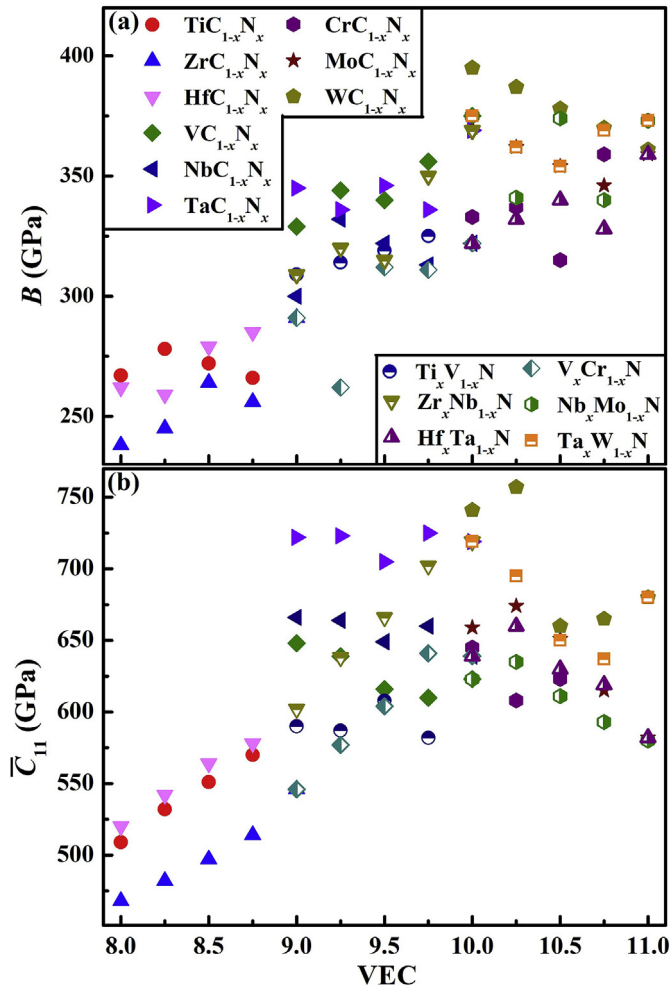
Fig. 4. (a) Bulk modulus B and (b) $\overline{C}_{11}$ of carbonitrides vs valence electron concentration VEC = 8–11.
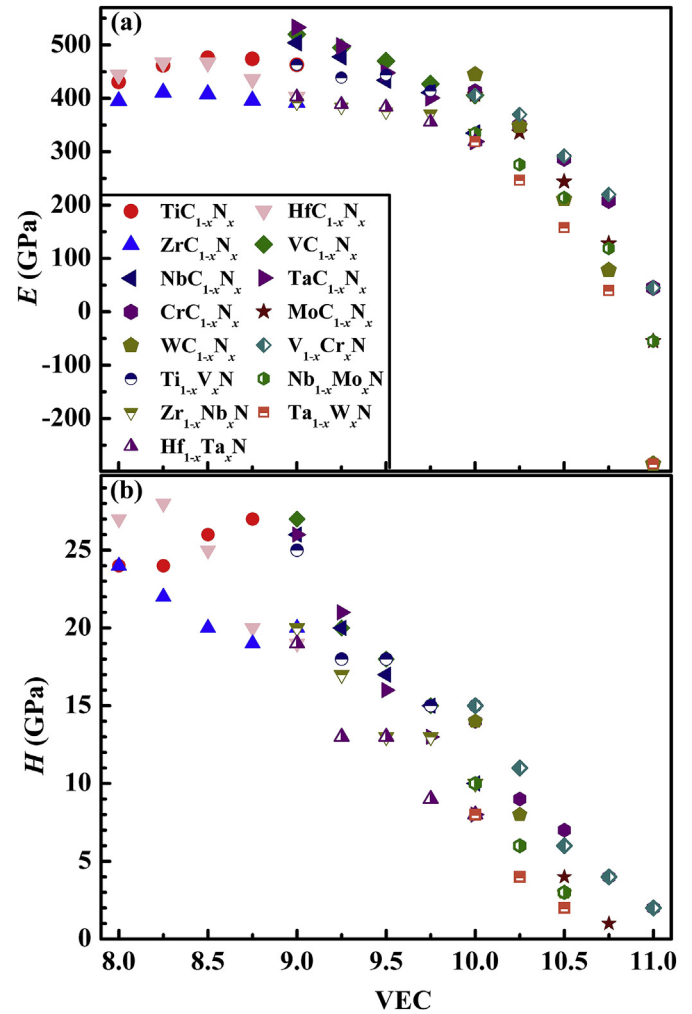
Fig. 5. (a) Elastic modulus E and (b) hardness H of carbonitrides and ternary nitrides vs valence electron concentration VEC = 8–11.

average 426 GPa for group 4 carbides at VEC = 8 to $E = 469$ GPa for VEC = 9, followed by a steep decrease to an average 234 GPa for VEC = 10.5 and −83 GPa for VEC = 11. The calculated elastic moduli are in excellent agreement (4–20% deviation) with the measured elastic moduli for early transition metal carbonitrides with VEC = 8–10 [21–23,100–102] but considerably (27–78%) deviate from the measured moduli for carbonitrides with VEC = 10–11 [26,36,37,103–106]. We attribute the deviations primarily to microstructural effects associated with residual stress in thin films as well as variations in composition, density and grain size. In addition, the presence of vacancies can significantly alter the mechanical properties for carbonitrides [100], most prominently if they are near mechanical instability such as group 6 nitrides [36,41,42,107]. Despite some deviations, the cited experimental reports confirm the calculated trend of decreasing elastic moduli with increasing VEC which is attributed to the increasing occupation of $d-t_{2g}$ orbitals as mentioned previously.

Fig. 5(b) is a plot of the Hardness H vs the VEC for carbonitrides and ternary nitrides, as determined from the calculated elastic tensor using Tian's model [73]. The data indicates that the hardness is similar (± 3 GPa) for different compounds that have the same VEC, but that H decreases with increasing VEC, showing a similar trend as $\overline{C}_{44}$ and E. More specifically, the average H decreases steeply from 25 GPa for group 4 carbides with VEC = 8 to $H = 4$ GPa at VEC = 10.5. For VEC > 10.5, the carbonitrides $MoC_{1-x}N_x$ and $WC_{1-x}N_x$

and the ternary nitrides $Nb_{1-x}Mo_xN$ and $Ta_{1-x}W_xN$ have no valid hardness because of their negative $\overline{C}_{44}$, while H of $V_{1-x}Cr_xN$ and $CrC_{1-x}N_x$ continues to decrease and reaches 2 GPa at VEC = 11. Comparing our hardness predictions in Fig. 5(b) with reported experimental nanoindentation data from epitaxial layers suggests that the agreement is relatively good (<25% deviation) for group 4 nitrides [21,100,101], but that the calculated hardness differs considerably (49–87% deviation) from experimentally measured values for binary nitrides, carbides and carbonitrides with VEC > 10 [23,37,103,106,108]. We attribute the deviations to residual stress, composition variations, vacancy concentrations, and crystalline defects in the experimental specimens, which are expected to be more dominant at higher VEC where the rocksalt structure may only be metastable and/or vacancies are energetically stable.

The dynamical stability of the binary nitrides and carbides of group 4–7 transition metals are explored by calculating the phonon dispersion curves as described in the procedure section. This is done because both dynamical and mechanical stability is necessary to determine the overall stability of the material. Imaginary frequencies near the Brillouin zone boundaries indicate dynamical instability, which may occur in some compounds despite that they are stable based on the static elastic stability criteria [109–111]. The nitrides of group 4 transition metals exhibit only real frequencies, indicating dynamical stability. In contrast, those for groups 5 and 6

also show some imaginary frequencies, that is, nitrides are unstable for VEC $\geq$ 10. That means, nitrides of group 5 are dynamically unstable despite that they are elastically stable. Similarly, the carbides are dynamically stable for groups 4 and 5 but unstable for group 6, corresponding to a dynamic instability for VEC $\geq$ 10, although they are elastically stable for group 6. In other words, a VEC of 10 is sufficient to cause dynamical instability in both binary carbides and nitrides while, in contrast, VEC >10.6 is required for elastic instability. A detailed quantitative determination of the critical VEC for dynamical instability is beyond the scope of the present work and is therefore not presented in this paper. We reiterate here that the mechanical stability of nitrides and carbides beyond VEC = 11 does not necessarily guarantee dynamical stability and that a systematic investigation of the phonon dispersion curves for mechanically stable binary nitrides and carbides with VEC >11 would be required.

Fig. 6 shows representative phonon dispersion curves from three nitrides, HfN, TaN and WN, corresponding to valence electron concentrations of 9, 10 and 11, respectively. The calculated phonon frequency f is plotted along high symmetry directions $\Gamma - X - W - K - \Gamma - L$ in the Brillouin zone, where frequencies below the dotted horizontal line $f = 0$ correspond to imaginary frequencies, indicating that a static displacement of atoms with the corresponding wavelength leads to an energy reduction. The phonon frequency of HfN is real throughout the Brillouin zone, with $f = 0-5$ and $12-17$ THz for the acoustic and optical branches, respectively, as shown by the navy-blue curves in Fig. 6. The longitudinal acoustic branch of the HfN dispersion curves shows anomalies along all three plotted high-symmetry $\Gamma - X$, $\Gamma - K$ and $\Gamma - L$ directions, corresponding to [100], [110] and [111] crystalline axes. For example, the branch along $\Gamma - X$ exhibits a softening near $q = 0.7$. Such softening has previously been reported for TiN [94,112], ZrN [94,113] and HfN [94,112,113] and has been attributed to the nesting of the Fermi surface in group 4 transition metal nitrides [114], leading to strong electron phonon coupling and a relatively high critical temperature for superconductivity [112,115]. Group 5 carbides have the same VEC = 9 as the group 4 nitrides and exhibit similar phonon spectra [94]. Hence, rocksalt structure nitrides and carbides with VEC = 9 exhibit fully real phonon spectra and are therefore dynamically stable up to their melting points.

The olive-green curve in Fig. 6 shows the vibrational frequencies for TaN, which has one valence electron more than HfN and belongs

to the group 5 nitrides with VEC = 10. The plot indicates the acoustic and optical branches to range from -6 to 3 THz and from 6 to 17 THz, respectively. The TaN optical modes extend over a wider frequency range than for HfN, resulting in some relatively soft optical phonon modes for TaN at approximately the middle between the zone center and boundary. More importantly, both the longitudinal and transversal acoustic branches exhibit imaginary frequencies at and near the X and K points of the Brillouin zone, including the path along the boundary from X to W to K. This is consistent with previous reports of the phonon spectra for the group 5 nitrides [94,114,116—118], and is attributed to the relatively high d-t_{2g} electron density near the Fermi level. Thus, displacement of neighboring cations in opposite directions promotes increased $d-t_{2g}$ orbital overlap and a corresponding energy reduction which results in dynamical instability [94,114,117,118]. The other nitrides and carbides with VEC = 10, namely group 5 nitrides and group 6 carbides, have qualitatively similar phonon dispersion curves as TaN. That is, they exhibit some imaginary frequencies and are therefore dynamically unstable despite that they are mechanically stable based on the calculated elastic tensor. However, we note here that finite temperature effects can stabilize these dynamically unstable branches as reported for VN [22,116].

Fig. 6 also shows the phonon dispersion curves for WN, representing the group 6 nitrides with VEC = 11, represented by the red curve. The optical phonon frequencies range from 9 to 18 THz and the acoustic phonons have a maximum frequency of 5 THz and a plotted minimum of -10 THz, indicating imaginary frequencies and dynamical instability, consistent with previously reported phonon dispersion curves of group 6 nitrides [94,113]. In contrast to TaN, the transverse acoustic branch for WN is imaginary for almost the entire Brillouin zone, indicating instability for phonons travelling along [100] and [110] directions for nearly all wavelengths. This is attributed to the instability of WN against shear along [100], as evident from the negative C_{44} presented in Figs. 2 and 3. This instability is due to the increasing overlap of d-t_{2g} orbitals which stabilize sheared structures with a reduced cation-cation distance along some of the $\langle 110 \rangle$ crystalline directions [41]. Nitrides and carbides with VEC = 11 could become dynamically stable at high temperatures. A systematic study needs to be done to verify this. We also note here that the elastic constants calculated at 0 K are still valid at finite temperatures because the phonon branches near the Γ point are not affected by temperature, as previously studied in detail for VN at various temperatures [116].

Effect of magnetization, Hubbard parameter, vacancies and temperature on the elastic constants and on the mechanical stability-instability transition:

There are various important parameters that have not been included in the above quantitative presentation of the mechanical properties of transition metal nitrides and carbides vs VEC. They have been neglected for consistency and simplicity purposes, but are discussed in the following, including the effect of the magnetization, the Hubbard parameter U, vacancies and the temperature. In order to explore the effect of magnetic ordering in nitrides and carbides containing Cr, Mn, Fe, Co, or Ni, spin-polarized calculations are performed to compare ferromagnetic and anti-ferromagnetic ordering with the non-magnetic structures. For these calculations, atomic positions are relaxed while forcing the overall structure to remain cubic, as explained in the procedure section. For the anti-ferromagnetic (AFM) structures, ordering along [100], [111] and [110] is considered. C_{44} calculations are performed on the lowest energy structure of each compound. Both CrN and MnN are found to be structurally stable in the [110] AFM configuration with C_{44} values of 126 and 122 GPa and with magnetic moments of 2.99

Fig. 6. Phonon dispersion curves of HfN, TaN and WN along high symmetry directions in the Brillouin zone. Imaginary frequencies are plotted as negative f values.

and 2.19 μ_B/cation, respectively, while their carbides are found to be stable in ferromagnetic configurations resulting in a C_{44} of 89 and 100 GPa with magnetic moments of 0.97 and 1.35 μ_B/cation, respectively. FeN is most stable in the ferromagnetic phase yielding $C_{44} = 69$ GPa with a magnetic moment of 2.29 μ_B/cation. CoN, CoC, NiN and NiC are non-magnetic. In summary, the spin-polarized calculations indicate that CrN, MnN, FeN are magnetically stabilized. The quantitative results are also included in the table provided as supplementary document.

The Hubbard parameter U can be used within DFT to account for on-site Coulomb repulsion, which can affect the mechanical properties due to the relatively localized d electrons in transition metal nitrides and carbides. For example, $U = 3$ eV for CrN has been reported to yield a $C_{44} = -116$ GPa [79,87], while the non-magnetic CrN with $U = 0$ in our study exhibits a positive $C_{44} = 8$ GPa. That is, Coulomb repulsion mechanically destabilizes CrN. Similarly, we expect Coulomb repulsion to reduce the mechanical stability of other compounds and envision that, as a consequence, all cubic nitrides and carbides with VEC $= 11-14$ are mechanically unstable, despite that some of them (CrN, CoN, MnC, FeC, RuC, and CoC) are predicted to be stable by our calculations with $U = 0$. This statement remains at this point speculative, since a detailed study of the effect of U on the mechanical stability is beyond the scope of this study, particularly because the determination of the most appropriate value for U for a given material is not well established.

Temperature is another parameter that affects the elastic constants and possibly also the critical VEC value for the stability-instability transition. Previous studies on the effect of temperature on the elastic constants C_{11}, C_{12} and B indicate that increasing temperature typically causes an increase in the lattice constants and a corresponding decrease in the bulk modulus and C_{11} and C_{12} [119–125]. This can be attributed to bond softening associated with the anharmonicity of the vibrational modes of atoms. In contrast, the relationship between $\overline{C}_{44}$ and the temperature is not as simple: For mechanically stable systems with a positive $\overline{C}_{44}$, temperature is expected to decrease $\overline{C}_{44}$, just like C_{11} and B [119–125]. However, for systems with a negative $\overline{C}_{44}$, increasing temperature could lead to augmentation of $\overline{C}_{44}$ because of the concave energy surface along directions of instability [126–128]. Thus, the effect of temperature on $\overline{C}_{44}$ is convoluted and high temperature calculations would need to be performed to accurately determine its effect. Nevertheless, we expect nitrides, carbides and carbonitrides with a VEC <11 to exhibit a $\overline{C}_{44}$ which decreases with increasing temperature while the temperature effect for the mechanically unstable structures remains uncertain.

Therefore, temperature may stabilize nitrides and carbides that exhibit a dynamical instability at 0 K. Such stabilization by temperature has previously been reported for the case of VN [116] and may also affect mechanical instability. Correspondingly, we expect temperature to reduce the magnitude of the slope in the $\overline{C}_{44}$ vs VEC plots in Figs. 2 and 3 by reducing $\overline{C}_{44}$ of the early transition metal carbonitrides and increasing $\overline{C}_{44}$ for the mechanically unstable structures with VEC $= 11-14$. This will also reduce the slopes of the E vs VEC and H vs VEC plots in Fig. 5, as E and H are strongly affected by changes in $\overline{C}_{44}$, as discussed above. Consequently, the critical VEC for mechanical instability is expected to increase with increasing temperature.

Vacancies on both cation and anion sublattices are common for most experimentally synthesized transition metal carbides [83,99,129,130] and nitrides [95,97,100,131–134] and are known to influence the crystal structure [25,26,107,135] as well as the electrical [136–138] and mechanical properties [36,41,44,100,139]. Vacancies in early rocksalt structure carbonitrides including HfN$_x$ and TiN$_x$ cause a softening of the elastic constant matrix and the elastic modulus [100,140,141]. However, for carbonitrides of group

6, vacancies are predicted to augment elastic constants and stabilize the rocksalt structure [25,41,142]. Thus, similar to temperature, vacancies are expected to reduce the slope of the elastic constants vs VEC plots, leading to an increase the critical VEC at which mechanical instability occurs. We note that this argument assumes that the VEC here is defined by the average number of electrons of the cations plus anions, neglecting the fact that vacancies themselves reduce the average number of electrons and therefore the VEC. This reduction in VEC through vacancies may in fact contribute to the stabilization of the rocksalt phase of e.g. group 6 nitrides, since a reduction in VEC leads to an increase in C_{44}, as shown in Figs. 2 and 3.

4. Conclusions

Calculated mechanical properties (ν, k, B, $\overline{C}_{11}$, $\overline{C}_{44}$, E, H) of rocksalt structure transition metal nitrides, carbonitrides and ternary nitrides indicate a steady increase in ductility with increasing VEC, with a brittleness-to-ductile transition at VEC $= 10$. The single crystal shear modulus $\overline{C}_{44}$ decreases from an average of 161 GPa for group 4 carbides to -39 GPa for group 6 nitrides, indicating a transition to mechanical instability at a critical valence electron concentration VEC $= 10.6$. In contrast, $\overline{C}_{11}$ increases from an average of 499 GPa for group 4 carbides to 681 and 614 GPa for group 5 and group 6 nitrides, while B increases over the same VEC $= 8-11$ range from an average of $B = 255-366$ GPa. The isotropic elastic modulus and hardness decrease steeply with increasing VEC. This is primarily attributed to the decreasing $\overline{C}_{44}$ which is caused by the increasing electron density in d-t_{2g} orbitals, resulting in an energy reduction upon shear and a corresponding softening with increasing VEC. Calculated phonon dispersion curves indicate a dynamical stability-instability transition between VEC $= 9$ and 10, which is below the critical VEC for mechanical instability of 10.6. Additionally, the mechanical stability is also affected by (i) magnetic ordering which stabilizes cubic CrN, MnN, FeN, (ii) on-site Coulomb repulsion which is accounted for by the Hubbard parameter and reduces the stability of compounds with an increasing VEC such that a considerable fraction of the d bands is filled, and (iii) temperature and point defects which both reduce $\overline{C}_{44} > 0$ and increase $\overline{C}_{44} < 0$, possibly causing an increase in the critical VEC for the stability-instability transition.

Acknowledgements

Appendix A. Supplementary data

Supplementary data related to this article can be found at https://doi.org/10.1016/j.actamat.2018.04.033.

References

[1] J. Musil, Hard and superhard nanocomposite coatings, Surf. Coating. Technol. 125 (2000) 322–330, https://doi.org/10.1016/S0257-8972(99)00586-1.

[2] K. Zhang, K. Balasubramanian, B.D. Ozsdolay, C.P. Mulligan, S.V. Khare, W.T. Zheng, D. Gall, Epitaxial NbCxN1-x(001) layers: growth, mechanical properties, and electrical resistivity, Surf. Coating. Technol. 277 (2015) 136–143, https://doi.org/10.1016/j.surfcoat.2015.07.025.

[3] H.S. Seo, T.Y. Lee, J.G. Wen, I. Petrov, J.E. Greene, D. Gall, Growth and physical properties of epitaxial HfN layers on MgO(001), J. Appl. Phys. 96 (2004) 878–884, https://doi.org/10.1063/1.1759783.

[4] S. Koseki, K. Inoue, S. Morito, T. Ohba, H. Usuki, Comparison of TiN-coated tools using CVD and PVD processes during continuous cutting of Ni-based

superalloys, Surf. Coating. Technol. 283 (2015) 353–363, https://doi.org/10.1016/j.surfcoat.2015.10.071.

[5] M. Yasuoka, P. Wang, R. Murakami, Comparison of the mechanical performance of cutting tools coated by either a TiCxN1−x single-layer or a TiC/TiC0.5N0.5/TiN multilayer using the hollow cathode discharge ion plating method, Surf. Coating. Technol. 206 (2012) 2168–2172, https://doi.org/10.1016/j.surfcoat.2011.09.053.

[6] E.E. Vera, M. Vite, R. Lewis, E.A. Gallardo, J.R. Laguna-Camacho, A study of the wear performance of TiN, CrN and WC/C coatings on different steel substrates, Wear 271 (2011) 2116–2124, https://doi.org/10.1016/j.wear.2010.12.061.

[7] Y.L. Su, T.H. Liu, Tribological properties of Ti2N-Wx% coatings deposited by magnetron sputtering, Vacuum 77 (2005) 343–354, https://doi.org/10.1016/j.vacuum.2004.12.004.

[8] X.Q. Chen, H. Niu, D. Li, Y. Li, Modeling hardness of polycrystalline materials and bulk metallic glasses, Intermetallics 19 (2011) 1275–1281, https://doi.org/10.1016/j.intermet.2011.03.026.

[9] C. Kral, W. Lengauer, D. Rafaja, P. Ettmayer, Critical review on the elastic properties of transition metal carbides, nitrides and carbonitrides, J. Alloy. Comp. 265 (1998) 215–233, https://doi.org/10.1016/S0925-8388(97)00297-1.

[10] L. Hultman, Thermal stability of nitride thin films, Vacuum 57 (2000) 1–30, https://doi.org/10.1016/S0042-207X(00)00143-3.

[11] B. Navinsek, S. Seal, Transition metal nitride functional coatings, JOM (J. Occup. Med.) 53 (2001) 51–54, https://doi.org/10.1007/s11837-001-0072-1.

[12] S. Jeon, J. Ha, Y. Choi, I. Jo, H. Lee, Interfacial stability and diffusion barrier ability of Ti1-xZrxN coatings by pulsed laser thermal shock, Appl. Surf. Sci. 320 (2014) 602–608, https://doi.org/10.1016/j.apsusc.2014.09.134.

[13] J.S. Becker, R.G. Gordon, Diffusion barrier properties of tungsten nitride films grown by atomic layer deposition from bis(tert-butylimido) bis(dimethylamido)tungsten and ammonia, Appl. Phys. Lett. 82 (2003) 2239–2241, https://doi.org/10.1063/1.1565699.

[14] M. Wittmer, TiN and TaN as diffusion barriers in metallizations to silicon semiconductor devices, Appl. Phys. Lett. 36 (1980) 456–458, https://doi.org/10.1063/1.91505.

[15] Z.T.Y. Liu, X. Zhou, D. Gall, S.V. Khare, First-principles investigation of the structural, mechanical and electronic properties of the NbO-structured 3d, 4d and 5d transition metal nitrides, Comput. Mater. Sci. 84 (2014) 365–373, https://doi.org/10.1016/j.commatsci.2013.12.038.

[16] C.S. Shin, D. Gall, P. Desjardins, A. Vailionis, H. Kim, I. Petrov, J.E. Greene, M. Odén, Growth and physical properties of epitaxial metastable cubic TaN(001), Appl. Phys. Lett. 75 (1999) 3808, https://doi.org/10.1063/1.125463.

[17] Z.T.Y. Liu, X. Zhou, S. V Khare, D. Gall, Structural, mechanical and electronic properties of 3d transition metal nitrides in cubic zincblende, rocksalt and cesium chloride structures: a first-principles investigation, J. Phys. Condens. Matter 26 (2014) 25404, https://doi.org/10.1088/0953-8984/26/2/025404.

[18] Z.T.Y. Liu, B.P. Burton, S.V. Khare, D. Gall, First-principles phase diagram calculations for the rocksalt-structure quasibinary systems TiN-ZrN, TiN-HfN and ZrN-HfN, J. Phys. Condens. Matter 29 (2017) 35401, https://doi.org/10.1088/0953-8984/29/3/035401.

[19] D. Gall, I. Petrov, N. Hellgren, L. Hultman, J.E. Sundgren, J.E. Greene, Growth of poly- and single-crystal ScN on MgO(001): role of low-energy N2+ irradiation in determining texture, microstructure evolution, and mechanical properties, J. Appl. Phys. 84 (1998) 6034–6041, https://doi.org/10.1063/1.368913.

[20] J.-E. Sundgren, Structure and properties of TiN coatings, Thin Solid Films 128 (1985) 21–44, https://doi.org/10.1016/0040-6090(85)90333-5.

[21] A.B. Mei, B.M. Howe, C. Zhang, M. Sardela, J.N. Eckstein, L. Hultman, A. Rockett, I. Petrov, J.E. Greene, Physical properties of epitaxial ZrN/MgO(001) layers grown by reactive magnetron sputtering, J. Vac. Sci. Technol., A 31 (2013) 61516, https://doi.org/10.1116/1.4825349.

[22] A.B. Mei, R.B. Wilson, D. Li, D.G. Cahill, A. Rockett, J. Birch, L. Hultman, J.E. Greene, I. Petrov, Elastic constants, Poisson ratios, and the elastic anisotropy of VN(001), (011), and (111) epitaxial layers grown by reactive magnetron sputter deposition, J. Appl. Phys. 115 (2014) 214908, https://doi.org/10.1063/1.4881817.

[23] K. Zhang, K. Balasubramanian, B.D. Ozsdolay, C.P. Mulligan, S.V. Khare, W.T. Zhang, D. Gall, Growth and physical properties of epitaxial NbN(001) films on MgO(001), Surf. Coating. Technol. 288 (2016) 105–114, https://doi.org/10.1016/j.surfcoat.2016.01.009.

[24] D. Gall, C.-S. Shin, T. Spila, M. Odén, M.J.H. Senna, J.E. Greene, I. Petrov, Growth of single-crystal CrN on MgO(001): effects of low-energy ion-irradiation on surface morphological evolution and physical properties, J. Appl. Phys. 91 (2002) 3589, https://doi.org/10.1063/1.1446239.

[25] B.D. Ozsdolay, K. Balasubramanian, D. Gall, Cation and anion vacancies in cubic molybdenum nitride, J. Alloy. Comp. 705 (2017) 631–637, https://doi.org/10.1016/j.jallcom.2017.02.072.

[26] B.D. Ozsdolay, C.P. Mulligan, K. Balasubramanian, L. Huang, S.V. Khare, D. Gall, Cubic β-WNx layers: growth and properties vs N-to-W ratio, Surf. Coating. Technol. 304 (2016) 98–107, https://doi.org/10.1016/j.surfcoat.2016.06.079.

[27] L. Rissanen, M. Neubauer, K.P. Lieb, P. Schaaf, The new cubic iron-nitride phase FeN prepared by reactive magnetron sputtering, J. Alloy. Comp. 274 (1998) 74–82, https://doi.org/10.1016/S0925-8388(98)00594-5.

[28] J.M. Córdoba, M.A. Avilés, M.J. Sayagués, M.D. Alcalá, F.J. Gotor, Synthesis of complex carbonitride powders TiyMT1-yCxN1-x (MT: Zr, V, Ta, Hf) via a mechanically induced self-sustaining reaction, J. Alloy. Comp. 482 (2009) 349–355, https://doi.org/10.1016/j.jallcom.2009.04.012.

[29] J. Ye, Y. Liu, H. Cao, Z. Weizhao, Z. Jiang, Z. Tang, A novel method to synthesize vanadium carbonitride nanopowders by thermal processing precursor, Int. J. Refract. Metals Hard Mater. 27 (2009) 858–861, https://doi.org/10.1016/j.ijrmhm.2009.04.002.

[30] W.F. Piedrahita, W. Aperador, J.C. Caicedo, P. Prieto, Evolution of physical properties in hafnium carbonitride thin fi lms, J. Alloy. Comp. 690 (2017) 485–496, https://doi.org/10.1016/j.jallcom.2016.08.109.

[31] E. Grigore, C. Ruset, X. Li, H. Dong, Zirconium carbonitride films deposited by combined magnetron sputtering and ion implantation (CMSII), Surf. Coating. Technol. 204 (2010) 1889–1892, https://doi.org/10.1016/j.surfcoat.2009.11.012.

[32] Y. Li, Y. Yao, W. Shao, F. Liu, Y. Kang, G. Yin, Z. Huang, X. Liao, Preparation of titanium carbonitride nanoparticles from a novel refluxing-derived precursor, Mater. Lett. 63 (2009) 1904–1906, https://doi.org/10.1016/j.matlet.2009.05.031.

[33] G. Abadias, V.I. Ivashchenko, L. Belliard, P. Djemia, Structure, phase stability and elastic properties in the Ti1−xZrxN thin-film system: experimental and computational studies, Acta Mater. 60 (2012) 5601–5614, https://doi.org/10.1016/j.actamat.2012.07.014.

[34] V.I. Ivashchenko, P.E.A. Turchi, V.I. Shevchenko, First-principles study of elastic and stability properties of ZrC − ZrN and ZrC − TiC alloys, J. Phys. Condens. Matter 21 (2009) 395503, https://doi.org/10.1088/0953-8984/21/39/395503.

[35] H. Kindlund, D.G. Sangiovanni, L. Martínez-De-Olcoz, J. Lu, J. Jensen, J. Birch, I. Petrov, J.E. Greene, V. Chirita, L. Hultman, Toughness enhancement in hard ceramic thin films by alloy design, Apl. Mater. 1 (2013) 42104, https://doi.org/10.1063/1.4822440.

[36] H. Kindlund, D.G. Sangiovanni, J. Lu, J. Jensen, V. Chirita, J. Birch, I. Petrov, J.E. Greene, L. Hultman, Vacancy-induced toughening in hard single-crystal V0.5Mo 0.5Nx/MgO(0 0 1) thin films, Acta Mater. 77 (2014) 394–400, https://doi.org/10.1016/j.actamat.2014.06.025.

[37] H. Kindlund, D.G. Sangiovanni, J. Lu, J. Jensen, V. Chirita, I. Petrov, J.E. Greene, L. Hultman, Effect of WN content on toughness enhancement in V1−xWxN/MgO(001) thin films, J. Vac. Sci. Technol., A 32 (2014) 30603, https://doi.org/10.1116/1.4867610.

[38] D.G. Sangiovanni, V. Chirita, L. Hultman, Toughness enhancement in TiAlN-based quaternary alloys, Thin Solid Films 520 (2012) 4080–4088, https://doi.org/10.1016/j.tsf.2012.01.030.

[39] D. Edstrom, D.G. Sangiovanni, L. Hultman, I. Petrov, J.E. Greene, V. Chirita, Elastic properties and plastic deformation of TiC- and VC-based pseudobinary alloys, Acta Mater. 144 (2018) 376–385, https://doi.org/10.1016/j.actamat.2017.10.047.

[40] M.J. Mehl, D. Finkenstadt, C. Dane, G.L.W. Hart, S. Curtarolo, Finding the stable structures of N1−xW x with an ab initio high-throughput approach, Phys. Rev. B 91 (2015) 184110, https://doi.org/10.1103/PhysRevB.91.184110.

[41] K. Balasubramanian, S. Khare, D. Gall, Vacancy-induced mechanical stabilization of cubic tungsten nitride, Phys. Rev. B 94 (2016) 174111, https://doi.org/10.1103/PhysRevB.94.174111.

[42] K. Balasubramanian, L. Huang, D. Gall, Phase stability and mechanical properties of Mo1-xNx with 0 ≤ x ≤ 1, J. Appl. Phys. 122 (2017) 195101, https://doi.org/10.1103/PhysRevB.82.054109.

[43] S.-H. Jhi, S. Louie, M. Cohen, J. Morris, Mechanical instability and ideal shear strength of transition metal carbides and nitrides, Phys. Rev. Lett. 87 (2001) 75503, https://doi.org/10.1103/PhysRevLett.87.075503.

[44] S.H. Jhi, S.G. Louie, M.L. Cohen, J. Ihm, Vacancy hardening and softening in transition metal carbides and nitrides, Phys. Rev. Lett. 86 (2001) 3348–3351, https://doi.org/10.1103/PhysRevLett.86.3348.

[45] S.-H. Jhi, J. Ihm, Electronic structure and structural stability of TiCxN1-x alloys, Phys. Rev. B 56 (1997) 13826, https://doi.org/10.1103/PhysRevB.56.13826.

[46] Z.T.Y. Liu, D. Gall, S.V. Khare, Electronic and bonding analysis of hardness in pyrite-type transition-metal pernitrides, Phys. Rev. B 90 (2014) 134102, https://doi.org/10.1103/PhysRevB.90.134102.

[47] H. Euchner, P.H. Mayrhofer, Vacancy-dependent stability of cubic and wurtzite Ti 1-x Al xN, Surf. Coating. Technol. 275 (2015) 214–218, https://doi.org/10.1016/j.surfcoat.2015.05.017.

[48] S. Guo, C. Ng, J. Lu, C.T. Liu, Effect of valence electron concentration on stability of fcc or bcc phase in high entropy alloys, J. Appl. Phys. 109 (2011) 103505, https://doi.org/10.1063/1.3587228.

[49] M. Pop, G. Borodi, S. Simon, Correlation between valence electron concentration and high-temperature superconductivity, J. Phys. Chem. Solid. 61 (2000) 1939–1944, https://doi.org/10.1016/S0022-3697(00)00084-6.

[50] D. Cherrad, M. Maouche, M. Maamache, L. Krache, Influence of valence electron concentration on elastic, electronic and optical properties of the alkaline-earth tin oxides A 3 SnO (A ¼ Ca, Sr and Ba): a comparative study with ASnO 3 compounds, Phys. B+C 406 (2011) 2714–2722, https://doi.org/10.1016/j.physb.2011.04.014.

[51] S.K.R. Patil, N.S. Mangale, S.V. Khare, S. Marsillac, Super hard cubic phases of period VI transition metal nitrides: first principles investigation, Thin Solid Films 517 (2008) 824–827, https://doi.org/10.1016/j.tsf.2008.07.034.

[52] J. Karthikeyan, V. Kumar, P. Murugan, The role of valance electron

concentration in tuning the structure, stability, and electronic properties of Mo6S9-xIx nanowires, J. Phys. Chem. C 119 (2015) 13979, https://doi.org/10.1021/acs.jpcc.5b04663.

[53] G. Soto, M.G. Moreno-Armenta, A. Reyes-Serrato, The role of valence electron concentration in the cohesive properties of YBxN1-x, YCxN1-x and YNxO1-x compounds, J. Alloy. Comp. 463 (2008) 559—563, https://doi.org/10.1016/j.jallcom.2007.09.114.

[54] H. Holleck, Material selection for hard coatings, J. Vac. Sci. Technol., A 4 (1986) 2661—2669, https://doi.org/10.1116/1.573700.

[55] D.G. Sangiovanni, L. Hultman, V. Chirita, Supertoughening in B1 transition metal nitride alloys by increased valence electron concentration, Acta Mater. 59 (2011) 2121—2134, https://doi.org/10.1016/j.actamat.2010.12.013.

[56] D.G. Sangiovanni, V. Chirita, L. Hultman, Electronic mechanism for toughness enhancement in TixM 1-xN M=Mo and W), Phys. Rev. B 81 (2010) 104107, https://doi.org/10.1103/PhysRevB.81.104107.

[57] Z. Wu, X. Chen, V. V Struzhkin, R.E. Cohen, Trends in elasticity and electronic structure of transition metal nitrides and carbides from first principles, Phys. Rev. B 71 (2005) 214103, https://doi.org/10.1103/PhysRevB.71.214103.

[58] H.W. Hugosson, U. Jansson, B. Johansson, O. Eriksson, Restricting dislocation movement in transition metal carbides by phase stability tuning, Science (80-). 293 (2001) 2434—2438, https://doi.org/10.1126/science.1060512.

[59] T. Joelsson, L. Hultman, H.W. Hugosson, J.M. Molina-Aldarguia, Phase stability tuning in the and enhanced mechanical strength thin-film system for large stacking fault density Phase stability tuning in the Nb x Zr 1 − x N thin-film system for large stacking fault density and enhanced mechanical strength, Appl. Phys. Lett. 86 (2005) 131922, https://doi.org/10.1063/1.1884743.

[60] D.G. Sangiovanni, L. Hultman, V. Chirita, I. Petrov, J.E. Greene, Effects of phase stability, lattice ordering, and electron density on plastic deformation in cubic TiWN pseudobinary transition-metal nitride alloys, Acta Mater. 103 (2016) 823—835, https://doi.org/10.1016/j.actamat.2015.10.039.

[61] F.F. Klimashin, P.H. Mayrhofer, Ab initio-guided development of super-hard Mo − Al − Cr − N coatings, Scripta Mater. 140 (2017) 27—30, https://doi.org/10.1016/j.scriptamat.2017.06.052.

[62] R. Rachbauer, D. Holec, P.H. Mayrhofer, Technology Increased thermal stability of Ti − Al − N thin films by Ta alloying, Surf. Coating. Technol. 211 (2012) 98—103, https://doi.org/10.1016/j.surfcoat.2011.07.009.

[63] G. Kresse, J. Hafner, Ab initio molecular dynamics for liquid metals, Phys. Rev. B 47 (1993) 558—561, https://doi.org/10.1103/PhysRevB.47.558.

[64] G. Kresse, J. Furthmüller, Efficient iterative schemes for ab initio total-energy calculations using a plane-wave basis set, Phys. Rev. B 54 (1996) 11169—11186, https://doi.org/10.1103/PhysRevB.54.11169.

[65] J.P. Perdew, K. Burke, M. Ernzerhof, Generalized gradient approximation made simple, Phys. Rev. Lett. 77 (1996) 3865—3868, https://doi.org/10.1103/PhysRevLett.77.3865.

[66] J. Perdew, J. Chevary, S. Vosko, K. Jackson, M. Pederson, D. Singh, C. Fiolhais, Erratum: atoms, molecules, solids, and surfaces: applications of the generalized gradient approximation for exchange and correlation, Phys. Rev. B 48 (1993), https://doi.org/10.1103/PhysRevB.48.4978.2, 4978—4978.

[67] A. Zunger, S.-H. Wei, L.G. Ferreira, J.E. Bernard, Special quasirandom structures, Phys. Rev. Lett. 65 (1990) 353. https://doi.org/10.1103/PhysRevLett.65.353.

[68] J. Pokluda, M. Černý, M. Šob, Y. Umeno, Ab initio calculations of mechanical properties: methods and applications, Prog. Mater. Sci. 73 (2015) 127—158, https://doi.org/10.1016/j.pmatsci.2015.04.001.

[69] M. Moakher, A.N. Norris, The closest elastic tensor of arbitrary symmetry to an elasticity tensor of lower symmetry, J. Elasticity 85 (2006) 215—263, https://doi.org/10.1007/s10659-006-9082-0.

[70] J. Paier, M. Marsman, K. Hummer, G. Kresse, I.C. Gerber, J.G. Angyán, Screened hybrid density functionals applied to solids, J. Chem. Phys. 124 (2006) 154709, https://doi.org/10.1063/1.2187006.

[71] R. Hill, The elastic behaviour of a crystalline aggregate, Proc. Phys. Soc. 65 (1952) 349—354, https://doi.org/10.1088/0370-1298/65/5/307.

[72] S.F. Pugh, Relations between the elastic moduli and the plastic properties of polycrystalline pure metals, Philos. Mag. Ser 45 (1954) 823—843, https://doi.org/10.1080/14786440808520496.

[73] Y. Tian, B. Xu, Z. Zhao, Microscopic theory of hardness and design of novel superhard crystals, Int. J. Refract. Metals Hard Mater. 33 (2012) 93—106, https://doi.org/10.1016/j.ijrmhm.2012.02.021.

[74] A. Togo, I. Tanaka, First principles phonon calculations in materials science, Scripta Mater. 108 (2015) 1—5, https://doi.org/10.1016/j.scriptamat.2015.07.021.

[75] D.G. Pettifor, Theoretical predictions of structure and related properties of intermetallics, Mater. Sci. Technol. 8 (1992) 345, https://doi.org/10.1179/mst.1992.8.4.345.

[76] Z.Q. Liu, W.H. Wang, M.Q. Jiang, Z.F. Zhang, Intrinsic factor controlling the deformation and ductile-to-brittle transition of metallic glasses, Phil. Mag. Lett. 94 (2014) 658—668, https://doi.org/10.1080/09500839.2014.955548.

[77] N. Shulumba, B. Alling, O. Hellman, E. Mozafari, P. Steneteg, M. Odén, I.A. Abrikosov, Vibrational free energy and phase stability of paramagnetic and antiferromagnetic CrN from ab initio molecular dynamics, Phys. Rev. B 89 (2014) 174108, https://doi.org/10.1103/PhysRevB.89.174108.

[78] A. Filippetti, W.E. Pickett, B.M. Klein, Competition between magnetic and structural transitions in CrN, Phys. Rev. B 59 (1999) 7043—7050, https://doi.org/10.1103/PhysRevB.59.7043.

[79] L. Zhou, F. Kormann, D. Holec, M. Bartosik, B. Grabowski, J. Neugebauer, P.H. Mayrhofer, Structural stability and thermodynamics of CrN magnetic phases from ab initio calculations and experiment, Phys. Rev. B 90 (2014) 184102, https://doi.org/10.1103/PhysRevB.90.184102.

[80] A. Filippetti, N.A. Hill, Magnetic stress as a driving force of structural Distortions : the case of CrN, Phys. Rev. Lett. 85 (2000) 5166, https://doi.org/10.1103/PhysRevLett.85.5166.

[81] J.A. Chan, J.Z. Liu, H. Raebiger, S. Lany, A. Zunger, Relative stability, electronic structure, and magnetism of MnN and (Ga,Mn)N alloys, Phys. Rev. B 78 (2008) 184109, https://doi.org/10.1103/PhysRevB.78.184109.

[82] B. Eck, R. Dronskowski, M. Takahashi, S. Kikkawa, Properties of binary 3D transition metal nitrides, J. Mater. Chem. 9 (1999) 1527—1537, https://doi.org/10.1039/A809935I.

[83] W. Olovsson, B. Alling, M. Magnuson, Structure and bonding in amorphous Cr 1−x C x nanocomposite thin films: X-ray absorption spectra and first-principles calculations, J. Phys. Chem. C 120 (2016) 12890—12899, https://doi.org/10.1021/acs.jpcc.6b03608.

[84] M.C. Qian, C.Y. Fong, L.H. Yang, Coexistence of localized magnetic moment and opposite-spin itinerant electrons in MnC, Phys. Rev. B 70 (2004) 52404, https://doi.org/10.1103/PhysRevB.70.052404.

[85] J.R. Frederick, J. D'Arcy-Gall, D. Gall, Growth of epitaxial CrN on MgO(001): role of deposition angle on surface morphological evolution, Thin Solid Films 494 (2006) 330—335, https://doi.org/10.1016/j.tsf.2005.08.244.

[86] L.M. Corliss, N. Elliott, J.M. Hastings, Antiferromagnetic structure of CrN, Phys. Rev. 117 (1960) 929—935, https://doi.org/10.1103/PhysRev.117.929.

[87] B. Alling, T. Marten, I.A. Abrikosov, Effect of magnetic disorder and strong electron correlations on the thermodynamics of CrN, Phys. Rev. B 82 (2010) 184430, https://doi.org/10.1103/PhysRevB.82.184430.

[88] S.-H. Jhi, J. Ihm, S.G. Louie, M.L. Cohen, Electronic mechanism of hardness enhancement in transition-metal carbonitrides, Nature 399 (1999) 132—134, https://doi.org/10.1038/20148.

[89] K. Bouamama, P. Djemia, D. Faurie, G. Abadias, Structural and elastic properties of single-crystal and polycrystalline Ti 1-xZr xN alloys: a computational study, J. Alloy. Comp. 536 (2012) S138—S142, https://doi.org/10.1016/j.jallcom.2011.12.034.

[90] K. Bouamama, P. Djemia, M. Benhamida, First-principles calculation of the structural and elastic properties of ternary metal nitrides TaxMo1-xN and TaxW1-xN, J. Phys. Conf. Ser 640 (2015) 12022, https://doi.org/10.1088/1742-6596/640/1/012022.

[91] D. Holec, F. Tasnádi, P. Wagner, M. Friák, J. Neugebauer, P.H. Mayrhofer, J. Keckes, Macroscopic elastic properties of textured ZrN-AlN polycrystalline aggregates: from ab initio calculations to grain-scale interactions, Phys. Rev. B 90 (2014) 1—9, https://doi.org/10.1103/PhysRevB.90.184106.

[92] D. Holec, M. Friak, J. Neugebauer, P.H. Mayrhofer, Trends in the elastic response of binary early transition metal nitrides, Phys. Rev. B 85 (2012) 64101, https://doi.org/10.1103/PhysRevB.85.064101.

[93] F. Tasnádi, I.A. Abrikosov, L. Rogström, J. Almer, M.P. Johansson, M. Oden, Significant elastic anisotropy in Ti1-x Alx N alloys, Appl. Phys. Lett. 97 (2010) 2008—2011, https://doi.org/10.1063/1.3524502.

[94] E.I. Isaev, S.I. Simak, I.A. Abrikosov, R. Ahuja, Y.K. Vekilov, M.I. Katsnelson, A.I. Lichtenstein, B. Johansson, Phonon related properties of transition metals, their carbides, and nitrides: a first-principles study, J. Appl. Phys. 101 (2007) 123519, https://doi.org/10.1063/1.2747230.

[95] D. Edström, D.G. Sangiovanni, L. Hultman, V. Chirita, Effects of atomic ordering on the elastic properties of TiN- and VN-based ternary alloys, Thin Solid Films 571 (2014) 145—153, https://doi.org/10.1016/j.tsf.2014.09.048.

[96] H. Kindlund, J. Lu, J. Jensen, I. Petrov, J.E. Greene, L. Hultman, Epitaxial V0.6W0.4N/MgO(001): evidence for ordering on the cation sublattice, J. Vac. Sci. Technol., A 31 (2013) 40602, https://doi.org/10.1116/1.4807654.

[97] F. Tian, J. D'Arcy-Gall, T.-Y. Lee, M. Sardela, D. Gall, I. Petrov, J.E. Greene, Epitaxial Ti[sub 1-x]W[sub x]N alloys grown on MgO(001) by ultrahigh vacuum reactive magnetron sputtering: electronic properties and long-range cation ordering, J. Vac. Sci. Technol., A 21 (2003) 140, https://doi.org/10.1116/1.1525818.

[98] A.I. Gusev, A.S. Kurlov, V.N. Lipatnikov, Atomic and vacancy ordering in carbide ζ-Ta4C3-x(0.28≤x≤0.40) and phase equilibria in the Ta-C system, J. Solid State Chem. 180 (2007) 3234—3246, https://doi.org/10.1016/j.jssc.2007.09.015.

[99] V.N. Lipatnikov, A.I. Gusev, P. Ettmayer, W. Lengauer, Phase transformations in non-stoichiometric vanadium carbide, J. Phys. Condens. Matter 11 (1999) 163—184, https://doi.org/10.1088/0953-8984/11/1/014.

[100] C.S. Shin, D. Gall, N. Hellgren, J. Patscheider, I. Petrov, J.E. Greene, Vacancy hardening in single-crystal TiNx(001) layers, J. Appl. Phys. 93 (2003) 6025—6028, https://doi.org/10.1063/1.1568521.

[101] H.S. Seo, T.Y. Lee, J.G. Wen, I. Petrov, J.E. Greene, D. Gall, Growth and physical properties of epitaxial HfN layers on MgO(001), J. Appl. Phys. 96 (2004) 878—884, https://doi.org/10.1063/1.1759783.

[102] Y. Sun, C. Lu, H. Yu, A. Kiet Tieu, L. Su, Y. Zhao, H. Zhu, C. Kong, Nano-mechanical properties of TiCN and TiCN/Ti coatings on Ti prepared by filtered arc deposition, Mater. Sci. Eng. 625 (2015) 56—64, https://doi.org/10.1016/j.msea.2014.11.093.

[103] S. Wang, X. Yu, J. Zhang, L. Wang, K. Leinenweber, D. He, Y. Zhao, Synthesis, hardness, and electronic properties of stoichiometric VN and CrN, Cryst. Growth Des. 16 (2016) 351—358, https://doi.org/10.1021/acs.cgd.5b01312.

[104] B.D. Ozsdolay, X. Shen, K. Balasubramanian, G. Scannell, L. Huang,

M. Yamaguchi, D. Gall, Elastic constants of epitaxial cubic Mon, Surf. Coating. Technol. 572 (2017) 1–17, https://doi.org/10.1016/j.surfcoat.2017.07.015.

[105] C.S. Shin, D. Gall, Y.W. Kim, P. Desjardins, I. Petrov, J.E. Greene, M. Odén, L. Hultman, Epitaxial NaCl structure δ-TaNx(001): electronic transport properties, elastic modulus, and hardness versus N/Ta ratio, J. Appl. Phys. 90 (2001) 2879–2885, https://doi.org/10.1063/1.1391214.

[106] P. Hones, N. Martin, M. Regula, F. Levy, Structural and mechanical properties of chromium nitride, molybdenum nitride, and tungsten nitride thin films, J. Phys. D Appl. Phys. 36 (2003) 1023–1029, https://doi.org/10.1088/0022-3727/36/8/313.

[107] F.F. Klimashin, N. Koutna, H. Euchner, D. Holec, P.H. Mayrhofer, The impact of nitrogen content and vacancies on structure and mechanical properties of Mo-N thin films, J. Appl. Phys. 120 (2016) 185301, https://doi.org/10.1063/1.4966664.

[108] B.D. Ozsdolay, C.P. Mulligan, M. Guerette, L. Huang, D. Gall, Epitaxial growth and properties of cubic WN on MgO(001), MgO(111), and Al2O3(0001), Thin Solid Films 590 (2015) 276–283, https://doi.org/10.1016/j.tsf.2015.08.002.

[109] D.M. Clatterbuck, C.R. Krenn, M.L. Cohen, J.W. Morris, Phonon instabilities and the ideal strength of aluminum, Phys. Rev. Lett. 91 (2003) 135501, https://doi.org/10.1103/PhysRevLett.91.135501.

[110] K. Persson, M. Ekman, V. Ozoliņš, Phonon instabilities in bcc Sc, Ti, La, and Hf, Phys. Rev. B 61 (2000) 11221–11224, https://doi.org/10.1103/PhysRevB.61.11221.

[111] K. Einarsdotter, B. Sadigh, G. Grimvall, V. Ozoliņs, Phonon instabilities in fcc and bcc tungsten, Phys. Rev. Lett. 79 (1997) 2073, https://doi.org/10.1103/PhysRevLett.79.5188.

[112] D. Gall, M. Stoehr, J.E. Greene, Vibrational modes in epitaxial Ti 1-x Sc x N (001) layers : an ab initio calculation and Raman spectroscopy study, Phys. Rev. B 64 (2001) 174302, https://doi.org/10.1103/PhysRevB.64.174302.

[113] B. Saha, J. Acharya, T.D. Sands, U.V. Waghmare, Electronic structure, phonons, and thermal properties of ScN, ZrN, and HfN: a first-principles study, J. Appl. Phys. 107 (2010) 33715, https://doi.org/10.1063/1.3291117.

[114] W. Weber, P. Roedhammer, L. Pintschovius, W. Reichardt, F. Gompf, A.N. Christensen, Phonon anomalies in VN and their electronic origin, Phys. Rev. Lett. 43 (1979) 868, https://doi.org/10.1103/PhysRevLett.43.868.

[115] A.B. Mei, A. Rockett, L. Hultman, I. Petrov, J.E. Greene, Electron/phonon coupling in group-IV transition-metal and rare-earth nitrides, J. Appl. Phys. 114 (2013) 193708, https://doi.org/10.1063/1.4832778.

[116] A.B. Mei, O. Hellman, N. Wireklint, C.M. Schleputz, D.G. Sangiovanni, B. Alling, A. Rockett, L. Hultman, I. Petrov, J.E. Greene, Dynamic and structural stability of cubic vanadium nitride, Phys. Rev. B 91 (2015) 54101, https://doi.org/10.1103/PhysRevB.91.054101.

[117] V.I. Ivashchenko, P.E.A. Turchi, E.I. Olifan, Phase stability and mechanical properties of niobium nitrides, Phys. Rev. B 82 (2010) 54109, https://doi.org/10.1016/j.ijhydene.2014.09.033.

[118] P. Rehák, M. Cerný, D. Holec, Interface-induced electronic structure toughening of nitride superlattices, Surf. Coating. Technol. 325 (2017) 410–416, https://doi.org/10.1016/j.surfcoat.2017.06.065.

[119] Y.P. Varshni, Temperature dependence of elastic constants, Phys. Rev. B 2 (1970) 3952–3957, https://doi.org/10.1103/PhysRevB.2.3952.

[120] P. Steneteg, O. Hellman, O. Vekilova, N. Shulumba, F. Tasnádi, P. Steneteg, O. Hellman, O. Vekilova, N. Shulumba, F. Tasnádi, P. Steneteg, O. Hellman, O.Y. Vekilova, N. Shulumba, F. Tasn, I.A. Abrikosov, Temperature dependence of TiN elastic constants from ab initio molecular dynamics simulations, Phys. Rev. B 87 (2013) 94114, https://doi.org/10.1103/PhysRevB.87.094114.

[121] A.J. Wang, S.L. Shang, Y. Du, Y. Kong, L.J. Zhang, L. Chen, D.D. Zhao, Z.K. Liu, Structural and elastic properties of cubic and hexagonal TiN and AlN from first-principles calculations, Comput. Mater. Sci. 48 (2010) 705–709, https://doi.org/10.1016/j.commatsci.2010.03.014.

[122] J.M. Dickinson, P.E. Armstrong, Temperature dependence of the elastic constants of molybdenum, J. Appl. Phys. 38 (1966) 602–605, https://doi.org/10.1063/1.1709381.

[123] A. Wang, S.L. Shang, M. He, Y. Du, L. Chen, R. Zhang, D. Chen, B. Fan, F. Meng, Z.K. Liu, Temperature-dependent elastic stiffness constants of fcc-based metal nitrides from first-principles calculations, J. Mater. Sci. 49 (2014) 424–432, https://doi.org/10.1007/s10853-013-7721-y.

[124] N. Shulumba, O. Hellman, L. Rogström, Z. Raza, F. Tasnádi, I.A. Abrikosov, M. Odén, Temperature-dependent elastic properties of Ti1-xAlxN alloys, Appl. Phys. Lett. 107 (2015), https://doi.org/10.1063/1.4936896.

[125] Y. Wang, J.J. Wang, H. Zhang, V.R. Manga, S.L. Shang, L.-Q. Chen, Z.-K. Liu, A first-principles approach to finite temperature elastic constants, J. Phys. Condens. Matter 22 (2010) 225404, https://doi.org/10.1088/0953-8984/22/22/225404.

[126] Q. Hong, S. Kadkhodaei, R. Sun, A. Van De Walle, The free energy of mechanically unstable phases, Nat. Commun. 6 (2015) 7559, https://doi.org/10.1038/ncomms8559.

[127] S. Kadkhodaei, Q. Hong, Free energy calculation of mechanically unstable but dynamically stabilized bcc titanium, Phys. Rev. B 95 (2017) 64101, https://doi.org/10.1103/PhysRevB.95.064101.

[128] J.C. Thomas, A. Van der Ven, Elastic properties and stress-temperature phase diagrams of high-temperature phases with low-temperature lattice instabilities, Phys. Rev. B 90 (2014) 224105, https://doi.org/10.1103/PhysRevB.90.224105.

[129] C.I. Sathish, Y. Guo, X. Wang, Y. Tsujimoto, J. Li, S. Zhang, Y. Matsushita, Y. Shi, H. Tian, H. Yang, J. Li, K. Yamaura, Superconducting and structural properties of δ-MoC 0.681 cubic molybdenum carbide phase, J. Solid State Chem. 196 (2012) 579–585, https://doi.org/10.1016/j.jssc.2012.07.037.

[130] L.V. Zueva, A.I. Gusev, Effect of nonstoichiometry and ordering on the period of the basis structure of cubic titanium carbide, Phys. Solid State 41 (1999) 1032–1038, https://doi.org/10.1134/1.1130931.

[131] A.J. Perry, On the existence of point defects in physical vapor deposited films of TiN, ZrN, and HfN, J. Vac. Sci. Technol., A 6 (1988) 2140, https://doi.org/10.1116/1.575205.

[132] R. Lamni, E. Martinez, S.G. Springer, R. Sanjines, P.E. Schmid, F. Levy, Optical and electronic properties of magnetron sputtered ZrNx thin films, Thin Solid Films 447–448 (2004) 316–321, https://doi.org/10.1016/S0040-6090.

[133] Z. Zhang, H. Li, R. Daniel, C. Mitterer, G. Dehm, Insights into the atomic and electronic structure triggered by ordered nitrogen vacancies in CrN, Phys. Rev. B 87 (2013) 14104, https://doi.org/10.1103/PhysRevB.87.014104.

[134] G.B. Smith, P.D. Swift, A. Bendavid, G.B. Smith, P.D. Swift, Films with metallic behavior at high N/Ti ratios for better solar control windows TiN x films with metallic behavior at high N/Ti ratios for better solar control windows, Appl. Phys. Lett. 630 (1999) 1–4, https://doi.org/10.1063/1.124463.

[135] H. Euchner, P.H. Mayrhofer, H. Riedl, F.F. Klimashin, A. Limbeck, P. Polcik, S. Kolozsvari, Solid solution hardening of vacancy stabilized Ti x W 1-x B 2, Acta Mater. 101 (2015) 55–61, https://doi.org/10.1016/j.actamat.2015.08.048.

[136] S. Kerdsongpanya, B. Alling, P. Eklund, Effect of point defects on the electronic density of states of ScN studied by first-principles calculations and implications for thermoelectric properties, Phys. Rev. B 86 (2012) 195140, https://doi.org/10.1103/PhysRevB.86.195140.

[137] R. Deng, B.D. Ozsdolay, P.Y. Zheng, S.V. Khare, D. Gall, Optical and transport measurement and first-principles determination of the ScN band gap, Phys. Rev. B 91 (2015) 45104, https://doi.org/10.1103/PhysRevB.91.045104.

[138] Z. Gu, C. Hu, X. Fan, L. Xu, M. Wen, Q. Meng, L. Zhao, X. Zheng, W. Zheng, On the nature of point defect and its effect on electronic structure of rocksalt hafnium nitride films, Acta Mater. 81 (2014) 315–325, https://doi.org/10.1016/j.actamat.2014.08.040.

[139] C. Hu, X. Zhang, Z. Gu, H. Huang, S. Zhang, X. Fan, W. Zhang, Q. Wei, W. Zheng, Negative effect of vacancies on cubic symmetry, hardness and conductivity in hafnium nitride films, Scripta Mater. 108 (2015) 141–146, https://doi.org/10.1016/j.scriptamat.2015.07.002.

[140] H.S. Seo, T.Y. Lee, I. Petrov, J.E. Greene, D. Gall, Epitaxial and polycrystalline Hf Nx (0.8≤x≤1.5) layers on MgO(001): film growth and physical properties, J. Appl. Phys. 97 (2005) 83521, https://doi.org/10.1063/1.1870097.

[141] T. Lee, K. Ohmori, C.S. Shin, D.G. Cahill, I. Petrov, J.E. Greene, Elastic constants of single-crystal Ti Nx (001) (0.67≤x≤1.0) determined as a function of x by picosecond ultrasonic measurements, Phys. Rev. B 71 (2005) 144106, https://doi.org/10.1103/PhysRevB.71.144106.

[142] N. Koutná, D. Holec, O. Svoboda, F.F. Klimashin, P.H. Mayrhofer, Point defects stabilise cubic Mo-N and Ta-N, J. Phys. D Appl. Phys. 49 (2016) 375303, https://doi.org/10.1088/0022-3727/49/37/375303.